

Geophysical Research Letters[®]



RESEARCH LETTER

10.1029/2024GL110510

Key Points:

- The nearside-farside asymmetry in mare basalt volcanic deposits has been attributed to thicker farside crust inhibiting eruption
- Challenging this hypothesis is the very deep, thin-crust ancient SPA impact basin, significantly underfilled by mare basalts
- After SPA impact-removal of insulating crust, sub-SPA lithosphere thickens anomalously early, inhibiting mare fill following cryptomaria

Supporting Information:

Supporting Information may be found in the online version of this article.

Correspondence to:

J. W. Head,
james_head@brown.edu






Citation:

Head, J. W., Wang, X., Lark, L. H., Wilson, L., & Qian, Y. (2024). Lunar nearside-farside mare basalt asymmetry: The combined role of global crustal thickness variations and South Pole-Aitken (SPA) basin-induced lithospheric thickening. *Geophysical Research Letters*, 51, e2024GL110510. <https://doi.org/10.1029/2024GL110510>

Received 10 JUN 2024

Accepted 16 OCT 2024

Lunar Nearside-Farside Mare Basalt Asymmetry: The Combined Role of Global Crustal Thickness Variations and South Pole-Aitken (SPA) Basin-Induced Lithospheric Thickening

James W. Head¹ , Xing Wang² , Laura H. Lark^{1,3} , Lionel Wilson⁴ , and Yuqi Qian⁵ 

¹Department of Earth, Environmental and Planetary Sciences, Brown University, Providence, RI, USA, ²Hong Kong Polytechnic University, Hong Kong, PR China, ³Institut de Physique du Globe de Paris, CNRS, Paris, France, ⁴Lancaster Environment Centre, Lancaster University, Lancaster, UK, ⁵The University of Hong Kong (HKU), Hong Kong, PR China

Abstract Lunar mare basalts represent melting of mantle material, buoyant ascent in dikes, and eruption onto <20% of the surface. Global mare distribution is distinctly asymmetrical, with a paucity on the farside, plausibly interpreted to be related to thicker farside low-density crust inhibiting buoyant magma rise to the surface. Challenging this hypothesis is the presence of the huge, ancient farside South Pole-Aitken (SPA) basin, site of the thinnest crust and deepest depression observed on the Moon. We hypothesize that an oblique impact stripped the farside crust within the SPA basin, permitting early mare basalt emplacement as cryptomaria due to thin/absent crust. However, removal of the SPA thermally insulating megaregolith/crust accelerated lithosphere thickening beneath the basin. This deepening rheological barrier inhibited buoyant rise of mantle diapirs below SPA, resulting in early abatement of mare basalt extrusions compared to the nearside, and retention of the deep, underfilled SPA impact basin observed today.

Plain Language Summary The cause of the observed asymmetry in nearside/farside mare basalt distribution (nearside ~15% of the surface, farside ~1%) has been attributed to differences in crustal thickness and the magma buoyancy at the base of the thicker crust, but this single factor is challenged by the presence of the ancient very deep SPA basin (average ~5 km), significantly underfilled by mare basalts compared to the nearside. We examine the effects of the formation of the giant (~2,300 km) SPA basin in removing the insulating megaregolith/crust, and show that it could first result in rapid cryptomaria emplacement due to near-absent crust, accompanied by enhanced heat loss within the basin, and formation of anomalously early thick sub-SPA lithosphere, inhibiting its mare filling due to a rheological barrier to basaltic magma eruptions, analogous to that which occurs later in lunar history on the lunar nearside.

1. Introduction

Luna 3 (1959) first lunar farside images revealed a substantial asymmetry in mare basalt deposits between the nearside (NS) and farside (FS) (Lipsky, 1965) (Figure 1c); many additional asymmetries have been documented: topography (Figure 1a), crustal thickness (Figure 1b), and compositional terrane types (Jolliff et al., 2000, 2006; Neal et al., 2023). Explanations for the mare basalt NS/FS asymmetry (Figure 1c) include: (a) asymmetric bombardment (Wood, 1973); (b) asymmetric degree-1 convection producing farside crustal thickening (Zhong et al., 2000); (c) South Pole-Aitken (SPA) basin impact (or other factors) reorganizing mantle and bringing heat-producing elements to NS Procellarum-KREEP Terrane (PKT) (Jones et al., 2022; Zhang et al., 2022); (d) formation of a huge nearside Procellarum impact basin thinning crust (Zhu et al., 2019); and so on. Many of these explanations imply significant variations in NS/FS crustal thickness (Figure 1b) and mantle heterogeneity, factors potentially causing, or contributing to, the NS/FS mare basalt asymmetry observed later in lunar history (Figure 1c). We first explore how the presence and thickness of a low-density anorthositic highland crust modulates the ascent and eruption of mare basalt magmas (Figure S1a-1 in Supporting Information S1), and thus their distribution on the lunar surface, and then address the effects of later lithospheric thickening (Figure S1a-2/3 in Supporting Information S1).

© 2024. The Author(s).

This is an open access article under the terms of the [Creative Commons Attribution-NonCommercial-NoDerivs License](https://creativecommons.org/licenses/by/4.0/), which permits use and distribution in any medium, provided the original work is properly cited, the use is non-commercial and no modifications or adaptations are made.

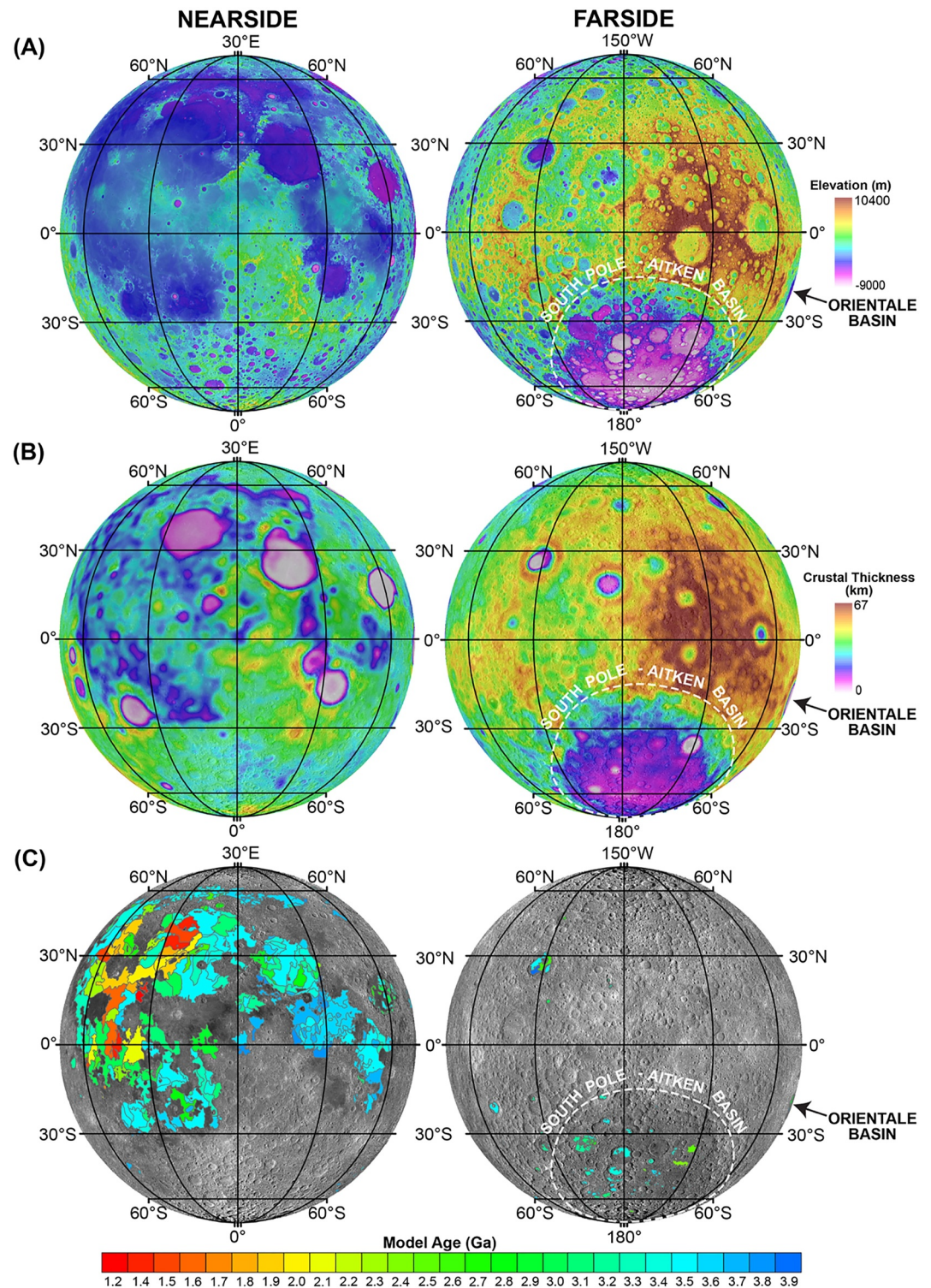


Figure 1. (a) Global topography (Smith et al., 2017). (b) Crustal thickness (M. Wiczeorek, 2012; Wiczeorek et al., 2013) (from GRAIL, Zuber et al., 2013); (c) Mare basalt distribution and ages (sources from Hiesinger et al., 2011, 2023); note that NS/FS mare basalt ages span a similar range, but farside basalts are less abundant.

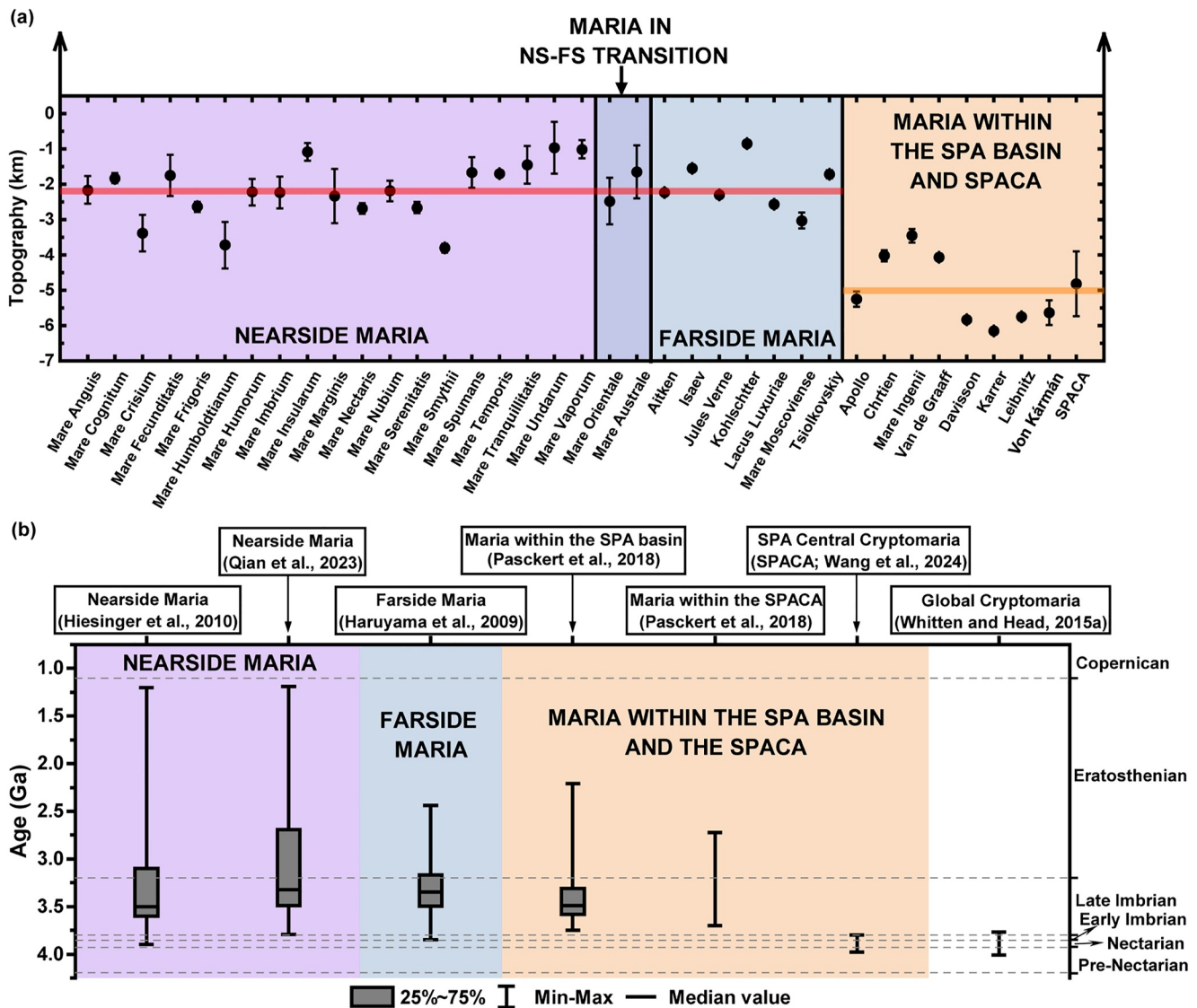


Figure 2. Average topography (a) and ages (b) of lunar global mare/cryptomare deposits and SPACA. The topographic values (Smith et al., 2017) in (a) are obtained by calculating the average value in each mare unit using mare boundaries from Nelson et al. (2014). The error bars represent the standard deviations of the topography distribution within individual mare regions. The maria/cryptomaria within SPA are highlighted by light-yellow background in (a). Clearly, SPA basin remains significantly underfilled relative to other lunar basins. (b) the ages of global mare/cryptomare deposits (Haruyama et al., 2009; Hiesinger et al., 2010, 2011; Pasckert et al., 2015; Qian et al., 2023; J. Whitten and Head, 2015a). Maria and cryptomaria within SPACA are highlighted by light-cyan background. This illustrates that the post-SPA-basin-formation cryptomare/mare deposits are continuous in the SPA basin center. Adapted from Wang et al. (2024).

2. Assessing the Role of Crustal Thickness

It has been hypothesized that the presence of low-density anorthositic crust plays a major role in inhibiting the ascent of magma in dikes, and extrusion of basalt onto the surface (e.g., Head et al., 2023; Head & Wilson, 1992, 2017; Wilson & Head, 1981, 2017, 2018a) (Figure S1a in Supporting Information S1). In this scenario, partial melting generates overpressure atop rising mantle diapirs, producing basalt magma-filled cracks (dikes) that ascend buoyantly toward the surface. Their ascent is modulated or halted by the presence of the low density anorthositic highlands crust. Relatively thicker (farside) crust further impedes eruption, whereas thinner nearside crust favors mare basalt emplacement (Figure S1b in Supporting Information S1). The ascent of mantle diapirs is controlled by the viscosity of the host rocks through which they rise. The buoyancy force driving the rise of a diapir containing partial melt increases slowly and linearly as the diapir moves upward and additional melting occurs. However, the effective viscosity of the surrounding rocks increases exponentially with decreasing depth

due to the decreasing temperature dictated by the geothermal gradient. Eventually the viscosity must dominate and the diapir rise speed must become very small. Also, as the temperature of the host rocks decreases with decreasing depth, the stress applied to them increases due to additional partial melting in the diapir. It is this combination that drives the host rocks from the plastic to the elastic regime, allowing a fracture to nucleate and partial melt to migrate out of the diapir into the growing dike. Thus, crustal thickness variations (Figure 1b), together with continuing thermal evolution resulting in increasing lithospheric thickness and a deepening rheological barrier to diapiric ascent (Figure S1 in Supporting Information S1), have been proposed as a first-order explanation for the global mare basalt NS/FS asymmetric distribution (Figure 1c) (Head & Wilson, 1992) and many of the characteristics of basaltic volcanism (Head & Wilson, 1992, 2017; Wilson & Head, 2017). This explanation requires no major difference in global mare basalt NS/FS mantle source regions; indeed, mare basalt ages on the NS/FS span a similar range, despite the lower abundance on the farside (Figure 1c).

Additional support for crustal thickness as a factor in mare basalt distribution was found in analysis of mare basalts in the Orientale basin on the western limb of the Moon, an area of transition between thinner NS crust (20–35 km) and thicker FS crust (35–60 km (Figure 1b). Whitten et al. (2011) confirmed the paucity of mare basalt deposits in Orientale, their occurrence primarily in the eastern, thinner-crust direction, and that their ages spanned the range of nearside mare basalts, again despite the lower basalt abundance (Figure 1). J. Whitten and Head (2015a,b) documented a global NS/FS asymmetric cryptomaria distribution, similar to that for maria. Further support for the role of crustal thickness was found in the distribution of floor-fractured craters (FFCs), interpreted to be intruded by shallow sills causing floor uplift and fracturing (Schultz, 1976). Detailed analysis of their distribution and characteristics (Jozwiak et al., 2012, 2015a, 2015b, 2017, 2015a) showed their concentration around the margins of nearside maria, in areas of transition from thinner nearside to thicker farside crust, and showed a distinct paucity on the farside, all factors consistent with models for the ascent and intrusion of mare basalts below crater floors in these marginal intermediate crustal thickness environments (Wilson & Head, 2018b).

3. The Challenge to Crustal Thickness as the Sole Explanation for NS/FS Mare Basalt Asymmetry

Despite the distinctive correlation (NS-thin crust, abundant maria; FS-thick crust, extreme paucity of maria) (Figure 1), Wieczorek et al. (2001) correctly pointed out that this hypothesis also predicts that the floor of the SPA basin, the site of the thinnest crust and deepest topography on the entire Moon (Figures 1a, 1b, and 2a) should be completely flooded to its rim in a manner similar to the NS Imbrium and Serenitatis basins (Figure 1c). Instead, although there is a concentration of mare patches on the SPA floor relative to the rest of the farside (Yingst & Head, 1997), and evidence for some ancient cryptomaria in the basin interior (Whitten and Head, 2015a, 2015b), SPA lacks the extensive fill predicted by the crustal thickness model alone, as shown by Wieczorek et al. (2001). Thus, although the general NS-FS crustal thickness/mare basalt distribution correlation remains, the underfilling of the SPA basin (Figures 1a and 1c, 2a) poses a serious challenge to crustal thickness as the sole factor in global maria distribution.

Recent comprehensive analysis of the interior of the SPA basin using a variety of remote sensing data has revealed the presence of significantly more cryptomaria on the floor of SPA than previously suspected (Figure 2b). Wang et al. (2024) showed evidence for a maximum cryptomaria area of $\sim 1.6 \times 10^5 \text{ km}^2$, corresponding to $\sim 2 \times 10^5 \text{ km}^3$ (a $>1\%$ volume increase in total global extrusive mare basalt volume); they concluded that, in a manner similar to nearside basins, SPA was a site of voluminous post-basin formation mare fill, but primarily in the form of early cryptomaria. Wang et al. (2024) found that the South Pole-Aitken Compositional Anomaly (SPACA) terrain (Moriarty & Pieters, 2018) is largely formed by ancient cryptomaria deposit emplacement following the formation of the SPA basin, and is interleaved with impact crater ejecta deposits (such as from the Apollo basin). On the basis of geological maps of superposed crater ages, they infer that the SPA central cryptomaria ages are no younger than Early Imbrian (about the time of the Orientale Basin event, 3.8 Ga (Yue et al., 2020); Figures 2a and 2b), an event that may also be responsible for the mantling of SPA maria to create the observed moderate-albedo cryptomaria, as is seen in most other lunar cryptomaria (Whitten and Head, 2015a, 2015b). Continued sparse post-Orientale mare basalt eruptions formed smaller patches in SPA (e.g., Morota et al., 2015; Paskert et al., 2015, 2018; Yingst & Head, 1997) whose albedo, spectral affinities, and early ages are similar to those of older nearside maria (Figures 1c and 2a, 2b).

Nevertheless, despite recent increased estimates of SPA basin interior cryptomare-mare volume (e.g., Wang et al., 2024; J. Whitten and Head, 2015a), SPA contains much less total mare material than that observed in nearside mare mascon basins (Figure 1c). The SPA basin interior remains anomalous in that it is characterized by the lowest topography (Figure 1a) and smallest regional crustal thickness (Figure 1b) on the Moon, and the least mare fill of all impact basins (Figures 2a and 2b).

4. The Nature of the South Pole-Aitken Basin Impact Event

We first outline the major setting and characteristics of the SPA basin, then utilize this framework to assess potential causes for the discrepancy between predictions and observations for the crustal thickness/lithospheric thickening NS/FS mare basalt asymmetry model (Head & Wilson, 2017; Wilson & Head, 2017). Large bolides impacting the Moon vertically or at high angles form deep transient cavities that remove the crust, potentially excavating and exposing the mantle (Melosh et al., 2017), and impart a significant amount of impact kinetic energy to the substrate, raising its temperature considerably. During the immediate collapse of the transient cavity, uplift of deeper, higher-temperature geotherms brings warmer material to the now-shallower basin floor (Bratt et al., 1985a, 1985b). The ponding of significant thicknesses of molten impact melt on the basin floor (e.g., Head, 1974; Vaughan et al., 2013) centralizes most of the material melted by the impact event. In contrast, low-angle impacts are characterized by shallower excavation, poor coupling of impact kinetic energy to the substrate, and much less production of impact melt (e.g., Anderson et al., 2003).

The SPA basin is the largest (~2,300 km) and oldest (~4.2–4.3 Ga; Ivanov et al., 2018) recognized basin on the Moon, formed by an oblique impact (Bill et al., 2024; Citron et al., 2024; Garrick-Bethell & Zuber, 2009; James et al., 2019; Melosh et al., 2017; Potter et al., 2012) into thick ancient anorthositic farside highland crust (Figures 1a and 1b). Evidence for the low angle of impact includes: the extreme SPA asymmetry; ejecta consist primarily of highland crustal material; evidence for little (Moriarty & Pieters, 2018) to no (Bill et al., 2024) highland crust remaining on the basin floor; and excavation of Th-rich basal crustal layers by post-SPA impacts (e.g., Garrick-Bethell & Zuber, 2005; Moriarty et al., 2021; Zhang et al., 2023), implying that the crust-mantle boundary is still preserved below parts of the SPA floor. Two aspects of the SPA impact are important: (a) the low impact angle minimized kinetic energy coupling and impact melt production/ponding, and (b) although low-angle impacts excavate proportionally less target material than high-angle impacts, the great size of SPA ensured efficient removal of almost all the insulating megaregolith and crust, resulting in enhanced cooling and lithospheric thickening.

5. Application to SPA Basin Mare Underfilling and the Nearside-farside Mare Basalt Asymmetry

On the basis of these characteristics, we propose the following qualitative scenario for SPA basin formation and evolution, mare underfilling and the nearside-farside mare basalt asymmetry (Figures 2a,b and 3): (a) At the time of the SPA impact, the lunar crust consisted of an upper, impact-produced megaregolith overlying an anorthositic crust, both thermally insulating layers (Paskert et al., 2018; Schumacher & Breuer, 2006; Warren & Rasmussen, 1987; Ziethe et al., 2009) with crustal thickness varying substantially between nearside and farside (Broquet and Andrews-Hanna, 2024a, 2024b) (Figures 1b and 3a). (b) The oblique SPA impact largely removed the ~60 km thick highland crust with its upper highly insulating megaregolith layer. (c) The SPA basin was so large and the lithosphere so thin that the steady-state configuration following rapid basin relaxation and cooling (~150 Ma) (Figure 3d) was isostatic, with no significant contribution from lithospheric rigidity, and thus no mascon was formed (Trowbridge et al., 2020). (d) The anomalously thin or absent crust on the SPA basin floor favored the eruption of mare basalts (Figure S1 in Supporting Information S1), resulting in the observed cryptomaria deposits (Figure 3b) (Wang et al., 2024; J. Whitten and Head, 2015a). (e) Concurrently, removal of the two major insulating layers (megaregolith and anorthositic crust) significantly enhanced the rate of heat loss from the SPA basin floor (Figure 3d) (e.g., Manga & Arkani-Hamed, 1991; Solomon et al., 1982; Ziethe et al., 2009); post-cryptomare volcanism concurrently waned to widely distributed mare patches (Figure 3c) (Paskert et al., 2018; Yingst & Head, 1997). (f) The enhanced cooling effect thickened the lithosphere below the SPA basin floor, an effect similar to the global thermal evolution trend (Figure 3d), but occurring locally and anomalously much earlier (e.g., Manga & Arkani-Hamed, 1991). (g) This anomalous thickening of SPA floor lithosphere (Figures 3c and 3d) inhibited the buoyant rise of mare basalt mantle diapirs (Figure S1 in Supporting Information S1), an effect usually observed later in the waning stages of global lunar thermal evolution (Figures 2 and 3d;

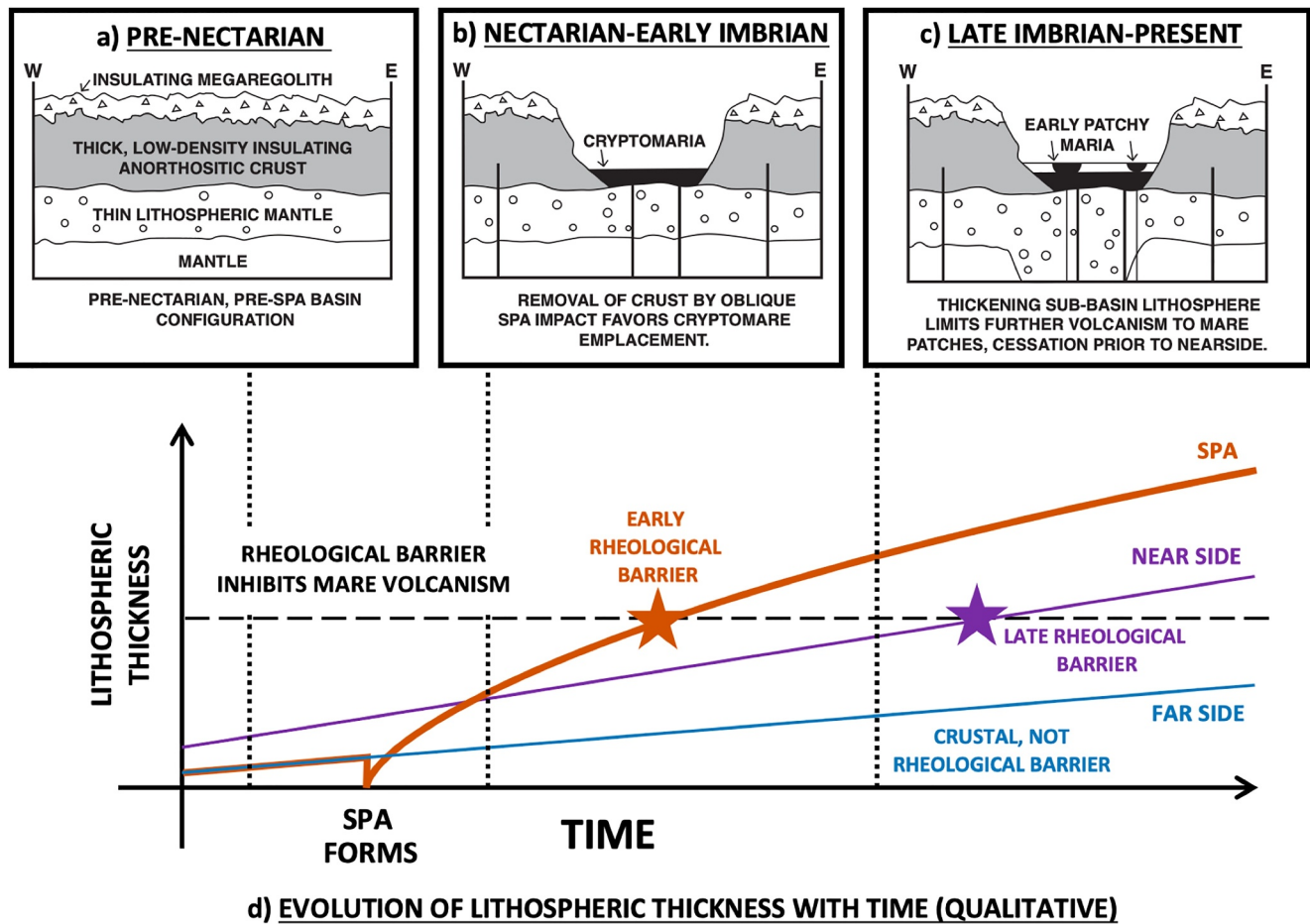


Figure 3. Diagrammatic representation of the sequence of events and timeline in the formation, thermal evolution and mare filling of the SPA basin. (a) Pre-SPA basin farside crust/lithospheric configuration. (b) Formation of SPA basin by an oblique impact produces anomalously thin to absent crust, favoring post-SPA basin cryptomaria emplacement due to removal of the megaregolith/crust density barrier. (c) Enhanced lithospheric thickening caused by megaregolith/anorthositic insulating crust removal results in waning of volcanism to smaller patches. By Late Imbrian, the lithosphere below the SPA floor has thickened sufficiently to cause cessation of volcanism on the SPA floor, and to preserve the anomalous setting (compared to the nearside) of limited volcanism in the thinnest crust and deepest topography of the Moon (Figure 3). (d) Qualitative sketch of lithospheric thickness over time beneath SPA, farside (thick crust highlands), and nearside (thin crust). Lithosphere beneath SPA thickens rapidly after removal of crust, reaching a thickness which suppresses the expression of mare basalts earlier than secular cooling results in the same thickness beneath the nearside. The lithosphere is thin under the farside, where the primary barrier to magma ascent is the thick crust.

Figure S1 in Supporting Information S1). (h) This effect resulted in an inhibition of basalt volcanism in post-Oriente, SPA basin floor-filling history, as evidenced by the transition from cryptomaria to mare patches (Figure 3c) and the ultimate cessation of eruptions there (Figure 1a) at a time of maximum nearside volcanic activity (Figures 1c and 2b). (i) The waning and ultimate cessation of SPA floor mare basalt volcanism further served to retain the anomalous depth (underfilled) and thin crust observed (e.g., Trowbridge et al., 2020) (Figures 1a, 1b, 2a, and 3c). This process may have occurred in similar impact basins on other planets but may not operate in the same manner given different target thermal properties, heat budgets and styles of mantle melt generation and eruption.

6. Assessing Quantitative Effects of Insulating Layer Removal and Temporal Implications

We next explore some basic heat conduction models to test the qualitative scenario outlined above (Figure 3) and to provide quantitative estimates of the timing and duration of the predicted phases of activity (Figure 4). We first outline a quantitative analysis of the effects of the removal of insulating layers and the temporal evolution related to changes in the geotherm migration and the effects on mantle mare basalt source region depths below the SPA basin interior as an assessment of the qualitative steps above (Figure 3).

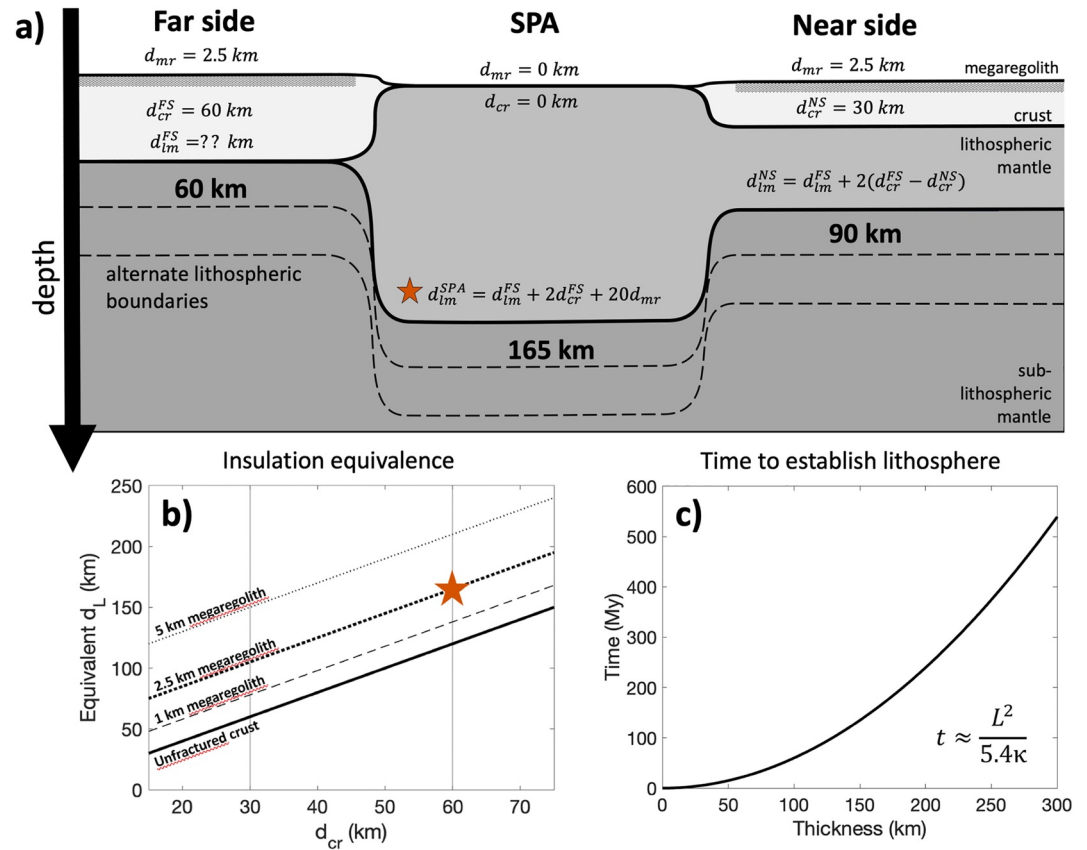


Figure 4. Thermal structure of the nearside and farside with the effects of the removal of the farside megaregolith and underlying anorthositic crust by the low-angle SPA basin impact. (a) Sketch of NS/FS and SPA lithospheric structure. (b) Lithospheric mantle thickness providing equivalent insulation to crustal layers. (c) Time to establish the lithosphere below SPA (megaregolith/crust removed).

The lunar lithosphere has three thermally important layers: the megaregolith, the underlying crust, and the lithospheric mantle. A 1-D model provides a reasonable approximation for the typical structure of these regions, which are much wider (e.g., 2,500 km diameter of SPA) than the thicknesses discussed (~ 300 km). We derive an expression for the importance of each layer using the 1-D steady-state heat equation with no volumetric heating:

$$\frac{d}{dz} \left(k \frac{dT}{dz} \right) = 0. \text{ Using a basal heat flux } q_b, \text{ integrating once gives } k \frac{dT}{dz} = -q_b. \text{ Integrating a second time gives}$$

$$T = -q_b \int_{z_0}^{z_1} \frac{1}{k} dz. \text{ With a system comprised of } n \text{ layers, each with thickness } d_i, \text{ and thermal conductivity } k_i, \text{ the}$$

integral simplifies to a sum, and we find that

$$\frac{\Delta T}{q_b} = \sum_{i=1}^n \frac{d_i}{k_i} \quad (1)$$

Equation 1 describes the insulating characteristics of different lithospheric structures; we now use it to estimate the lithospheric thickness below SPA and compare it to the nearside (Figure 4). If we assume that the base of the lithosphere is defined by a surface of constant temperature and constant heat flux, as is approximately true in stagnant lid convection, the left hand side of Equation 1 is approximately constant when describing the lithosphere, demonstrating that the contribution of each layer to the insulation of the interior is defined by its thickness divided by its thermal conductivity. The thermal conductivities of the megaregolith, crust, and lithospheric mantle are approximately $0.2 \text{ W m}^{-1} \text{ K}^{-1}$, $2 \text{ W m}^{-1} \text{ K}^{-1}$, and $4 \text{ W m}^{-1} \text{ K}^{-1}$, respectively (Maurice et al., 2020; Zhang et al., 2013a, 2013b); in other words, the lithospheric mantle is 20 times as thermally conductive as the megaregolith and 2 times as thermally conductive as the unfractured crust. The steady-state lithospheric thickness

beneath SPA must provide at least the same insulation as the removed crust and megaregolith. If the SPA-forming impact removed 2.5 km of megaregolith and 60 km of crust, then after thermal equilibrium was reached the thermal effect of 2.5 km of megaregolith would be replaced by that of 50 km of lithospheric mantle (20 \times ; a net increase in thickness of 47.5 km), while the 57.5 km of unfractured crust would be replaced by 115 km of lithospheric mantle (2 \times ; a net increase of 57.5 km) for a total net lithospheric thickening of 105 km. Similarly, compared to SPA, the lunar nearside lithospheric mantle must be thinner than the farside by 75 km due to the insulation of the \sim 27.5 km crust and 2.5 km megaregolith.

Heat-producing elements (HPE) in the crust or lithosphere would necessitate even greater lithospheric thickening beneath SPA to achieve equivalent basal lithospheric heat flux. With an additional thin sub-crustal layer producing heat at rate H W/m², the above translations between removed crustal material and increased lithospheric thicknesses increase by a factor of $F_H = 1 + H/q_b$ (Section S1 in Supporting Information S1). If heat production and basal heat flux are approximately equal, plausible if the layer contains about half of the Moon's HPE, the net lithospheric thickening under SPA would be nearly 300 km.

Additional lateral heterogeneities in the thermal structure of the lunar lithosphere have been hypothesized. Nearside basal heat flux may be higher if the nearside deep mantle is enriched in HPE, perhaps by 50% (Laneuville et al., 2018). Furthermore, the SPA impact itself generated a thermal anomaly, with a thick melt sheet and large thermal imprint. Although the melt sheet contained significant heat, this heat would be lost quickly due to effective heat transport in partially molten bodies (Vaughan et al., 2013); with no atmosphere, even planet-scale magma oceans reach near-solidus in 100,000 years (Elkins-Tanton, 2008). However, the deeper thermal imprint due to impact heating and isotherm uplift may have affected the longer-term thermal and convective state. Models of mantle evolution following a vertical impact (Jones et al., 2022) or oblique (Zhang et al., 2022) impact predict a long-lived (>500 My) warm plume under SPA (though the long-term consequences of an oblique impact at different angles (e.g., Citron et al., 2024) should be further explored). These predictions best describe convection in the sublithospheric mantle; lithospheric basal heat flux and mantle-surface temperature contrast may be on the order of 10%–20% larger under SPA, similar (but opposite) in magnitude to expected latitude-based variations. If the sublithospheric heat flux and mantle-surface temperature contrast at SPA differ by a factor of F_q and F_T , respectively, the estimated lithospheric mantle thicknesses would change by a factor of F_T/F_q (Section S2 in Supporting Information S1).

Thus, removal of crust and megaregolith by the SPA-forming impact should eventually lead to substantial lithospheric thickening. Furthermore, the value of lithosphere thickness beneath SPA in Figure 4 (165 km) is an approximate lower bound; if HPE are preferentially located in the deep crust and/or nearside mantle, the true value may be much larger. This lithosphere will grow over time, in a manner similar to the lithosphere beneath new spreading oceanic crust on Earth. With a half-space cooling model, which works well to describe the early growth of the lithosphere on Earth (Davis & Lister, 1974), the time to establish a lithosphere with thickness L will be approximately $t = \frac{L^2}{(2 \operatorname{erf}^{-1}(\Delta T_L/\Delta T_M))^2 \kappa}$, where κ is the thermal diffusivity (10^{-6} m²/s is an approximate value for the lunar lithosphere (cf. Zhang et al., 2013a, 2013b) and $\Delta T_L/\Delta T_M$ is the temperature difference across the lithosphere, normalized by the mantle-surface temperature difference; $\Delta T_L/\Delta T_M = 0.9$ gives $(2 \operatorname{erf}^{-1}(\Delta T_L/\Delta T_M))^2 = 5.4$. The growth of a lithosphere to be 150–300 km thick would take approximately 130–530 million years (Figure 4c). Consistent with these timing predictions is the presence of the initial peak phase of cryptomare emplacement in the SPA basin interior (Lark et al., 2024; Wang et al., 2024) (Figure 2b), rapidly waning to isolated mare patches and then ceasing altogether relative to the lunar nearside (Figure 1c).

7. Conclusions

On the basis of our analysis, we find that a plausible explanation for the observed first-order NS/FS mare basalt asymmetry (Figure 1c) involves: 1) the effect of the thicker low-density anorthositic crustal density trap (Figure S1a in Supporting Information S1) inhibiting rising basaltic magmas from reaching the surface on the farside, compared with the thinner crust on the nearside (Figures 1b and 3a; Figure S1b in Supporting Information S1), combined with 2) the subsequent evolutionary thickening of the lithosphere and the onset of the importance of lithospheric buoyancy traps at greater depths (Figures 3b and 3c; Figure S1 in Supporting Information S1), as originally envisioned (Head & Wilson, 1992). We conclude that the observed anomalous depth and mare basalt underfilling of the farside SPA basin (Wieczorek et al., 2001) can be accounted for by the efficient large-scale

removal of the megaregolith-crust mantle-insulating layers by the SPA oblique impact event. This resulted in enhanced heat loss on the basin floor, locally producing a region of lithosphere which thickened anomalously early (Figures 3c and 3d), serving to preferentially deepen the rheological trap to rising mantle diapirs below SPA (Fig. S1 in Supporting Information S1). This thickening caused the waning and cessation of SPA basin floor volcanism prior to the late Imbrian peak phase of lunar nearside volcanism (Figures 1c, 2c, 3c, and 3d). The SPA basin subsequently remained topographically deep (Figures 1a and 2a) and underfilled compared with the lunar nearside (Figures 1c, 2b and 3d), as observed today. The recent success of the Chang'e-6 mission, which returned 1,935.3 g of lunar samples from the SPA/Apollo basin farside mare basalts (Li et al., 2024; Qian et al., 2024), may soon enable further tests of this hypothesis.

Data Availability Statement

The LOLA elevation (https://astrogeology.usgs.gov/search/map/moon_lro_lola_dem_118m) and global LROC WAC image (https://astrogeology.usgs.gov/search/map/moon_lro_lroc_wac_global_morphology_mosaic_100m) are available through USGS Astropedia. The shapefile of Hiesinger et al. (2011)'s mare unit model ages is available through the LROC website (https://wms.lroc.asu.edu/lroc/view_rdr/SHAPEFILE_HIESINGER2011_MARE_AGE_UNITS).

Acknowledgments

The authors declare no real or perceived financial conflicts of interests.

References

- Anderson, J. L., Schultz, P. H., & Heineck, J. T. (2003). Asymmetry of ejecta flow during oblique impacts using three-dimensional particle image velocimetry. *Journal of Geophysical Research: Planets*, 108(E8). <https://doi.org/10.1029/2003je002075>
- Bill, C. A., Collins, G. C., Davison, T. M., Baijal, N., & Kim, D. (2024). Constraining impact parameters for the South Pole-Aitken basin, LPSC 54. *Abstract*, 2007.
- Bratt, S. R., Solomon, S. C., & Head, J. W. (1985). The evolution of impact basins: Cooling, subsidence, and thermal stress. *Journal of Geophysical Research*, 90(B14), 12415–12433. <https://doi.org/10.1029/jb090ib14p12415>
- Bratt, S. R., Solomon, S. C., Head, J. W., & Thurber, C. H. (1985). The deep structure of lunar basins: Implications for basin formation and modification. *Journal of Geophysical Research*, 90(B4), 3049–3064. <https://doi.org/10.1029/jb090ib04p03049>
- Broquet, A., & Andrews-Hanna, J. C. (2024a). The Moon before mare. *Icarus*, 408, 115846.
- Broquet, A., & Andrews-Hanna, J. C. (2024b). A volcanic inventory of the Moon. *Icarus*, 411, 115954. <https://doi.org/10.1016/j.icarus.2024.115954>
- Citron, R. I., Smith, D. E., Stewart, S. T., Hood, L. L., & Zuber, M. T. (2024). The South Pole-Aitken basin: Constraints on impact excavation, melt, and ejecta. *Geophysical Research Letters*, 51(14), e2024GL110034. <https://doi.org/10.1029/2024gl110034>
- Davis, E. E., & Lister, C. R. B. (1974). Fundamentals of ridge crest topography. *Earth and Planetary Science Letters*, 21(4), 405–413. [https://doi.org/10.1016/0012-821x\(74\)90180-0](https://doi.org/10.1016/0012-821x(74)90180-0)
- Elkins-Tanton, L. T. (2008). Linked magma ocean solidification and atmospheric growth for Earth and Mars. *Earth and Planetary Science Letters*, 271(1–4), 181–191.
- Garrick-Bethell, I., & Zuber, M. T. (2005). An indigenous origin for the South Pole Aitken basin thorium anomaly. *Geophysical research letters*, 32(13). <https://doi.org/10.1029/2005gl023142>
- Garrick-Bethell, I., & Zuber, M. T. (2009). Elliptical structure of the lunar South Pole-Aitken basin. *Icarus*, 204(2), 399–408. <https://doi.org/10.1016/j.icarus.2009.05.032>
- Haruyama, J., Ohtake, M., Matsunaga, T., Morota, T., Honda, C., Yokota, Y., et al. (2009). Long-lived volcanism on the lunar farside revealed by SELENE Terrain Camera. *Science*, 323(5916), 905–908. <https://doi.org/10.1126/science.1163382>
- Head, J. W. (1974). Orientale multi-ringed basin interior and implications for the petrogenesis of lunar highland samples. *The Moon*, 11(3–4), 327–356. <https://doi.org/10.1007/bf00589168>
- Head, J. W., & Wilson, L. (1992). Lunar mare volcanism: Stratigraphy, eruption conditions, and the evolution of secondary crusts. *Geochimica et Cosmochimica Acta*, 56(6), 2155–2175. [https://doi.org/10.1016/0016-7037\(92\)90183-j](https://doi.org/10.1016/0016-7037(92)90183-j)
- Head, J. W., & Wilson, L. (2017). Generation, ascent and eruption of magma on the Moon: New insights into source depths, magma supply, intrusions and effusive/explosive eruptions (Part 2: Predicted emplacement processes and observations). *Icarus*, 283, 176–223. <https://doi.org/10.1016/j.icarus.2016.05.031>
- Head, J. W., Wilson, L., Hiesinger, H., Van Der Bogert, C., Chen, Y., Dickson, J. L., et al. (2023). Lunar mare basaltic volcanism: Volcanic features and emplacement processes. *Reviews in Mineralogy and Geochemistry*, 89(1), 453–507. <https://doi.org/10.2138/rmg.2023.89.11>
- Hiesinger, H., Van Der Bogert, C. H., Michael, G., Schmedemann, N., Iqbal, W., Robbins, S. J., Ivanov, B., et al. (2023). The lunar cratering chronology. *Reviews in Mineralogy and Geochemistry*, 89(1), 401–451. <https://doi.org/10.2138/rmg.2023.89.10>
- Hiesinger, H., Head, J. W., III, Wolf, U., Jaumann, R., & Neukum, G. (2010). Ages and stratigraphy of lunar mare basalts in Mare Frigoris and other nearside maria based on crater size-frequency distribution measurements. *Journal of Geophysical Research*, 115(E3). <https://doi.org/10.1029/2009JE003380>
- Hiesinger, H., Head, J. W., Wolf, U., Jaumann, R., & Neukum, G. (2011). Ages and stratigraphy of lunar mare basalts: A synthesis. In: Recent advances and current research issues in lunar stratigraphy. Ambrose WA, Williams DA (eds). *Geological Society of America Special Paper*, 477, 1–51.
- Ivanov, M. A., Hiesinger, H., Van Der Bogert, C. H., Orgel, C., Pasckert, J. H., & Head, J. W. (2018). Geologic history of the northern portion of the South Pole-Aitken basin on the Moon. *Journal of Geophysical Research: Planets*, 123(10), 2585–2612. <https://doi.org/10.1029/2018je005590>
- James, P. B., Smith, D. E., Byrne, P. K., Kendall, J. D., Melosh, H. J., & Zuber, M. T. (2019). Deep structure of the lunar South Pole-Aitken basin. *Geophysical Research Letters*, 46(10), 5100–5106. <https://doi.org/10.1029/2019gl082252>

- Jolliff, B. L., Gillis, J. J., Haskin, L. A., Korotev, R. L., & Wieczorek, M. A. (2000). Major lunar crustal terranes: Surface expressions and crust-mantle origins. *Journal of Geophysical Research*, 105(E2), 4197–4216. <https://doi.org/10.1029/1999je001103>
- Jolliff, B. L., Wieczorek, M. A., Shearer, C. K., & Neal, C. R. (Eds.) (2006). *New views of the moon, reviews in mineralogy & geochemistry*, 60.
- Jones, M. J., Evans, A. J., Johnson, B. C., Weller, M. B., Andrews-Hanna, J. C., Tikoo, S. M., & Keane, J. T. (2022). A South Pole–Aitken impact origin of the lunar compositional asymmetry. *Science Advances*, 8(14), eabm8475. <https://doi.org/10.1126/sciadv.abm8475>
- Jozwiak, L. M., Head, J. W. III, Neumann, G. A., & Wilson, L. (2015a). The effect of evolving gas distribution on shallow lunar magmatic intrusion density: Implications for gravity anomalies. *Lunar Planet Science Conference*, 46, 1580.
- Jozwiak, L. M., Head, J. W., III, Neumann, G. A., & Wilson, L. (2017). Observational constraints on the identification of shallow lunar magmatism: Insights from floor-fractured craters. *Icarus*, 283, 224–231. <https://doi.org/10.1016/j.icarus.2016.04.020>
- Jozwiak, L. M., Head, J. W., III, & Wilson, L. (2015b). Lunar floor-fractured craters as magmatic intrusions: Geometry, modes of emplacement, associated tectonic and volcanic features, and implications for gravity anomalies. *Icarus*, 248, 424–447. <https://doi.org/10.1016/j.icarus.2014.10.052>
- Jozwiak, L. M., Head, J. W., III, Zuber, M. T., Smith, D. E., & Neumann, G. A. (2012). Lunar floor-fractured craters: Classification, distribution, origin and implications for magmatism and shallow crustal structure. *Journal of Geophysical Research*, 117(E11). <https://doi.org/10.1029/2012je004134>
- Laneville, M., Taylor, J., & Wieczorek, M. A. (2018). Distribution of radioactive heat sources and thermal history of the Moon. *Journal of Geophysical Research: Planets*, 123(12), 3144–3166. <https://doi.org/10.1029/2018je005742>
- Lark, L. H., Huber, C., Parmentier, E. M., & Head, J. W. (2024). Planetary interior configuration control on thermal evolution and geological history. *Journal of Geophysical Research: Planets*, 129, e2024JE008361. <https://doi.org/10.1029/2024JE008361>
- Li, C., Hu, H., Yang, M. F., Liu, J., Zhou, Q., Ren, X., et al. (2024). Nature of the lunar farside samples returned by the Chang'E-6 mission. *National Science Review*, nwae328.
- Lipsky, Y. N. (1965). Zond-3 photographs of the Moon's far side. *Sky and Telescope*, 30, 338.
- Manga, M., & Arkani-Hamed, J. (1991). Remelting mechanisms for shallow source regions of mare basalts. *Physics of the Earth and Planetary Interiors*, 68(1–2), 9–31. [https://doi.org/10.1016/0031-9201\(91\)90003-z](https://doi.org/10.1016/0031-9201(91)90003-z)
- Maurice, M., Tosi, N., Schwinger, S., Breuer, D., & Kleine, T. (2020). A long-lived magma ocean on a young Moon. *Science Advances*, 6(28), eaba8949. <https://doi.org/10.1126/sciadv.aba8949>
- Melosh, H. J., Kendall, J., Horgan, B., Johnson, B. C., Bowling, T., Lucey, P. G., & Taylor, G. J. (2017). South Pole–Aitken basin ejecta reveal the Moon's upper mantle. *Geology*, 45(12), 1063–1066. <https://doi.org/10.1130/g39375.1>
- Moriarty, D. P., & Pieters, C. M. (2018). The character of South Pole–Aitken Basin: Patterns of surface and subsurface composition. *Journal of Geophysical Research: Planets*, 123(3), 729–747. <https://doi.org/10.1002/2017je005364>
- Moriarty, D. P., Watkins, R. N., Valencia, S. N., Kendall, J. D., Evans, A. J., Dygert, N., & Petro, N. E. (2021). Evidence for a stratified upper mantle preserved within the south pole–Aitken Basin. *Journal of Geophysical Research: Planets*, 121(1), e2020JE006589. <https://doi.org/10.1029/2020JE006589>
- Morota, T., Ishihara, Y., Sasaki, S., Goossens, S., Matsumoto, K., Noda, H., et al. (2015). Lunar mare volcanism: Lateral heterogeneities in volcanic activity and relationship with crustal structure, in *Volcanism and Tectonism across the Inner Solar System*, ed. by T. Platz, M. Massironi, P. K. Byrne, & H. Hiesinger. *Geological Society, London Special Publications*, 401(1), 127–138. <https://doi.org/10.1144/SP401.11>
- Neal, C. R., Gaddis, L. R., Jolliff, B. L., Lawrence, S. J., Mackwell, S. J., Shearer, C. K., & Valencia, S. N. (2023). New views of the Moon 2.
- Nelson, D. M., Koeber, S. D., Daud, K., Robinson, M. S., Watters, T. R., Banks, M. E., & Williams, N. R. (2014). Mapping lunar maria extents and lobate scarps using LROC image products. *45th Annual Lunar and Planetary Science Conference (No. 1777)*, 2861.
- Pasckert, J. H., Hiesinger, H., & Van Der Bogert, C. H. (2015). Small-scale lunar farside volcanism. *Icarus*, 257, 336–354. <https://doi.org/10.1016/j.icarus.2015.04.040>
- Pasckert, J. H., Hiesinger, H., & Van Der Bogert, C. H. (2018). Lunar farside volcanism in and around the South Pole–Aitken basin. *Icarus*, 299, 538–562. <https://doi.org/10.1016/j.icarus.2017.07.023>
- Potter, R. W., Collins, G. S., Kiefer, W. S., McGovern, P. J., & Kring, D. A. (2012). Constraining the size of the South Pole–Aitken basin impact. *Icarus*, 220(2), 730–743. <https://doi.org/10.1016/j.icarus.2012.05.032>
- Qian, Y., Head, J., Michalski, J., Wang, X., Van Der Bogert, C., Hiesinger, H., et al. (2024). Long-lasting farside volcanism in the Apollo basin: China's Chang'e-6 landing site. *Earth and Planetary Science Letters*, 637, 118737. <https://doi.org/10.1016/j.epsl.2024.118737>
- Qian, Y., She, Z., He, Q., Xiao, L., Wang, Z., Head, J. W., et al. (2023). Mineralogy and chronology of the young mare volcanism in the Procellarum–KREEP–Terrane. *Nature Astronomy*, 7(3), 287–297. <https://doi.org/10.1038/s41550-022-01862-1>
- Schultz, P. H. (1976). Floor-fractured lunar craters. *The Moon*, 15(3–4), 241–273. <https://doi.org/10.1007/Bf00562240>
- Schumacher, S., & Breuer, D. (2006). Influence of a variable thermal conductivity on the thermo-chemical evolution of Mars. *Journal of Geophysical Research Planets*, 111(E2). <https://doi.org/10.1029/2005je002429>
- Smith, D. E., Zuber, M. T., Neumann, G. A., Mazarico, E., Lemoine, F. G., Head, J. W., III, et al. (2017). Summary of the results from the lunar orbiter laser altimeter after seven years in lunar orbit. *Icarus*, 283, 70–91. <https://doi.org/10.1016/j.icarus.2016.06.006>
- Solomon, S. C., Comer, R. P., & Head, J. W. (1982). The evolution of impact basins: Viscous relaxation of topographic relief. *Journal of Geophysical Research*, 87(B5), 3975–3992. <https://doi.org/10.1029/jb087ib05p03975>
- Trowbridge, A. J., Johnson, B. C., Freed, A. M., & Melosh, H. J. (2020). Why the lunar South Pole–Aitken Basin is not a mascon. *Icarus*, 352, 113995. <https://doi.org/10.1016/j.icarus.2020.113995>
- Vaughan, W. M., Head, J. W., Wilson, L., & Hess, P. C. (2013). Geology and petrology of enormous volumes of impact melt on the Moon: A case study of the Orientale basin impact melt sea. *Icarus*, 223(2), 749–765. <https://doi.org/10.1016/j.icarus.2013.01.017>
- Wang, X., Head, J. W., Chen, Y., Zhao, F., Kreslavsky, M. A., Wilson, L., et al. (2024). Lunar farside South Pole Aitken basin interior: Evidence for more extensive central cryptomaria in the South Pole–Aitken compositional anomaly (SPACA). *Journal of Geophysical Research: Planets*, 129(5), e2023JE008176. <https://doi.org/10.1029/2023je008176>
- Warren, P., & Rasmussen, K. (1987). Megaregolith insulation, internal temperatures, and bulk uranium content of the Moon. *Journal of Geophysical Research*, 92(B5), 3453–3465. <https://doi.org/10.1029/jb092ib05p03453>
- Whitten, J., Head, J. W., III, Staid, C. M., Staid, M. I., Pieters, C. M., Mustard, J. F., et al. (2011). Lunar mare deposits associated with the Orientale impact basin: New insights into mineralogy, history, mode of emplacement, and relation to Orientale Basin evolution from Moon Mineralogy Mapper (M3) data from Chandrayaan-1. *Journal of Geophysical Research*, 116, E00G09. <https://doi.org/10.1029/2010JE003736>
- Whitten, J. L., & Head, III, J. W. (2015a). Lunar cryptomaria: Physical characteristics, distribution, and implications for ancient volcanism. *Icarus*, 247, 150–171. <https://doi.org/10.1016/j.icarus.2014.09.031>
- Whitten, J. L., & Head, J. W., III. (2015b). Lunar cryptomaria: Mineralogy and composition of ancient volcanic deposits. *Planetary and Space Science*, 106, 67–81. <https://doi.org/10.1016/j.pss.2014.11.027>

- Wieczorek, M. (2012). GRAIL crustal thickness archive [dataset]. *Zenodo*. <https://doi.org/10.5281/zenodo.997347>
- Wieczorek, M. A., Neumann, G. A., Nimmo, F., Kiefer, W. S., Taylor, G. J., Melosh, H. J., et al. (2013). The crust of the Moon as seen by GRAIL. *Science*, 339(6120), 671–675. <https://doi.org/10.1126/science.1231530>
- Wieczorek, M. A., Zuber, M. T., & Phillips, R. J. (2001). The role of magma buoyancy on the eruption of lunar basalts. *Earth and Planetary Science Letters*, 185(1–2), 71–83. [https://doi.org/10.1016/S0012-821X\(00\)00355-1](https://doi.org/10.1016/S0012-821X(00)00355-1)
- Wilson, L., & Head, J. W. (2017). Generation, ascent and eruption of magma on the Moon: New insights into source depths, magma supply, intrusions and effusive/explosive eruptions (Part 1: Theory). *Icarus*, 283, 146–175. <https://doi.org/10.1016/j.icarus.2015.12.039>
- Wilson, L., & Head, J. W. (2018a). Controls on lunar basaltic volcanic eruption structure and morphology: Gas release patterns in sequential eruption phases. *Geophysical Research Letters*, 45(12), 5852–5859. <https://doi.org/10.1029/2018gl078327>
- Wilson, L., & Head, J. W., III. (1981). Ascent and eruption of basaltic magma on the Earth and Moon. *Journal of Geophysical Research*, 86(B4), 2971–3001. <https://doi.org/10.1029/jb086ib04p02971>
- Wilson, L., & Head, J. W. III. (2018b). Lunar floor-fractured craters: Modes of dike and sill emplacement and implications of gas production and intrusion cooling on surface morphology and structure. *Icarus*, 305, 105–122. <https://doi.org/10.1016/j.icarus.2017.12.030>
- Wood, J. A. (1973). Bombardment as a cause of the lunar asymmetry. *The Moon*, 8(1), 73–103. <https://doi.org/10.1007/bf00562751>
- Yingst, R. A., & Head, J. W., III. (1997). Volumes of lunar lava ponds in South Pole-Aitken and Orientale basins: Implications for eruption conditions, transport mechanisms, and magma source regions. *Journal of Geophysical Research*, 102(E5), 10909–10931. <https://doi.org/10.1029/97je00717>
- Yue, Z., Yang, M., Jia, M., Michael, G., Di, K., Gou, S., & Liu, J. (2020). Refined model age for Orientale Basin derived from zonal crater dating of its ejecta. *Icarus*, 346, 113804. <https://doi.org/10.1016/j.icarus.2020.113804>
- Zhang, J., Head, J. W., Liu, J., & Potter, R. W. (2023). Lunar Procellarum KREEP terrane (PKT) stratigraphy and structure with depth: Evidence for significantly decreased Th concentrations and thermal evolution consequences. *Remote Sensing*, 15(7), 1861. <https://doi.org/10.3390/rs15071861>
- Zhang, N., Ding, M., Zhu, M. H., Li, H., Li, H., & Yue, Z. (2022). Lunar compositional asymmetry explained by mantle overturn following the South Pole–Aitken impact. *Nature Geoscience*, 15(1), 37–41. <https://doi.org/10.1038/s41561-021-00872-4>
- Zhang, N., Parmentier, E. M., & Liang, Y. (2013a). Effects of lunar cumulate mantle overturn and megaregolith on the expansion and contraction history of the Moon. *Geophysical Research Letters*, 40(19), 5019–5023. <https://doi.org/10.1002/grl.50988>
- Zhang, N., Parmentier, E. M., & Liang, Y. (2013b). A 3-D numerical study of the thermal evolution of the Moon after cumulate mantle overturn: The importance of rheology and core solidification. *Journal of Geophysical Research: Planets*, 118(9), 1789–1804. <https://doi.org/10.1002/jgre.20121>
- Zhong, S., Parmentier, E. M., & Zuber, M. T. (2000). A dynamic origin for the global asymmetry of lunar mare basalts. *Earth and Planetary Science Letters*, 177(3–4), 131–140. [https://doi.org/10.1016/S0012-821X\(00\)00041-8](https://doi.org/10.1016/S0012-821X(00)00041-8)
- Zhu, M. H., Wünnemann, K., Potter, R. W., Kleine, T., & Morbidelli, A. (2019). Are the Moon's nearside-farside asymmetries the result of a giant impact? *Journal of Geophysical Research: Planets*, 124(8), 2117–2140. <https://doi.org/10.1029/2018je005826>
- Zieth, R., Seiferlin, K., & Hiesinger, H. (2009). Duration and extent of lunar volcanism: Comparison of 3D convection models to mare basalt ages. *Planetary and Space Science*, 57(7), 784–796. <https://doi.org/10.1016/j.pss.2009.02.002>
- Zuber, M. T., Smith, D. E., Watkins, M. M., Asmar, S. W., Konopliv, A. S., Lemoine, F. G., et al. (2013). Gravity field of the Moon from the gravity recovery and interior laboratory (GRAIL) mission. *Science*, 339(6120), 668–671. <https://doi.org/10.1126/science.1231507>